Biogeosciences Discuss., 10, 8159–8201, 2013
www.biogeosciences-discuss.net/10/8159/2013/
doi:10.5194/bgd-10-8159-2013

Biogeosciences Discussions
Open Access

Microbial activity and carbonate isotope signatures as a tool for identification of spatial differences in methane advection: a case study at the Pacific Costa Rican margin

S. Krause[1], P. Steeb[1], C. Hensen[1], V. Liebetrau[1], A. W. Dale[1], M. Nuzzo[2], and T. Treude[1]

[1]GEOMAR Helmholtz Centre for Ocean Research Kiel, Wischhofstr. 1–3, 24148 Kiel, Germany
[2]LNEG, Marine Geology Department, Alfragide, Portugal & Instituto Dom Luiz, University of Lisbon, Lisbon, Portugal

Received: 29 March 2013 – Accepted: 16 April 2013 – Published: 15 May 2013

Correspondence to: S. Krause (skrause@geomar.de) and T. Treude (ttreude@geomar.de)

Published by Copernicus Publications on behalf of the European Geosciences Union.

Abstract

Subduction of the oceanic Cocos plate offshore Costa Rica causes strong advection of methane-charged fluids. Presented here are the first direct measurements of microbial anaerobic oxidation of methane (AOM) and sulfate reduction (SR) rates in sediments from the two mounds, applying radiotracer techniques in combination with numerical modeling. In addition, analysis of carbonate $\delta^{18}O$, $\delta^{13}C$, and $^{87}Sr/^{86}Sr$ signatures constrain the origin of the carbonate-precipitating fluid. Average rates of microbial activities showed differences with a factor of 4.8 to 6.3 between Mound 11 [AOM 140.71 (±40.84 SD); SR 117.25 (±82.06 SD) mmol m^{-2} d^{-1}, respectively] and Mound 12 [AOM 22.37 (±0.85 SD); SR 23.99 (±5.79 SD) mmol m^{-2} d^{-1}, respectively]. Modeling results yielded flow velocities of 50 cm a^{-1} at Mound 11 and 8–15 cm a^{-1} at Mound 12. Analysis of oxygen and carbon isotope variations of authigenic carbonates from the two locations revealed higher values for Mound 11 ($\delta^{18}O$: 4.7 to 5.9‰, $\delta^{13}C$: −21.0 to −29.6‰), compared to Mound 12 ($\delta^{18}O$: 4.1 to 4.5‰, $\delta^{13}C$: −45.7 to −48.9‰). Analysis of carbonates $^{87}Sr/^{86}Sr$ indicated temporal changes of deep-source fluid admixture at Mound 12. The present study is in accordance with previous work supporting considerable differences of methane flux between the two Mounds. It also strengthens the hypothesis of a predominantly deep fluid source for Mound 11 versus a rather shallow source of biogenic methane for Mound 12. The results demonstrate that methane-driven microbial activity is a valid ground truthing tool for geophysical measurements of fluid advection and constraining of recent methane fluxes in the study area. The study further shows that the combination of microbial rate measurements, numerical modeling, and authigenic carbonate analysis provide a suitable approach to constrain temporal and spatial variations of methane charged fluid flow at the Pacific Costa Rican margin.

BGD
10, 8159–8201, 2013

1 Introduction

Areas of oceanic plate subduction represent sites of convection driven by the down welling of the oceanic plate below the continental plate, an essential process for geochemical cycling between the crust and the mantle. Along with oceanic crust material, water and volatiles are subducted into the mantle. During the decent, these components are exposed to increasing pressure and temperature, causing alteration of the chemical (Manning, 2004) and isotopic signatures (Ellam and Hawkesworth, 1988). As a result of hydraulic pressure increase, porewater buoyancy, diagenetic and higher metamorphic mineral reaction, dewatering processes, as well as upward directed fluid flow can be observed in the area of the fore arc (Scambelluri et al., 2007).

During the ascent, fluids become charged with encountered elements, ions and gasses. When these fluids exit the sediment surface, they represent what is commonly known as cold seeps. Cold seep systems can be associated with different geological formations such as crater-like structures (pockmarks) or mud extrusions (mounds, volcanoes) (Judd et al., 2002). These systems are often characterized by authigenic carbonate concretions of micritic crystal morphology (Naehr et al., 2007), produced by microbial **a**naerobic **o**xidation of **m**ethane (AOM) in the sediment (e.g. Bohrmann et al., 1998; Greinert et al., 2001; Suess, 2010).

The prerequisite for microbial related authigenic carbonates at cold seeps is the advection of methane (CH_4). In marine sediments, methane is formed either as the result of microbial (biogenic methane) or thermal (thermogenic methane) degradation of organic matter (Schoell, 1988; Thauer, 1998). Thermogenic methanogenesis is either facilitated by (1) pyrolysis of organic matter or (2) water-rock interaction, resulting in different carbon isotope signatures.

In anoxic sediments, methane removal is mediated by microbial sulfate (SO_4^{2-})-dependent AOM (Boetius et al., 2000). The general reaction of AOM is (Barnes and Goldberg, 1976):

$$CH_4 + SO_4^{2-} \rightarrow HCO_3^- + HS^- + H_2O \quad (1)$$

BGD
10, 8159–8201, 2013

AOM and **s**ulfate **r**eduction (SR) increase porewater alkalinity, producing bicarbonate (HCO_3^-), which can dissociates into carbonate (CO_3^{2-}). In case of supersaturation, carbonate minerals may form, predominantly with Ca^{2+} ions (Peckmann et al., 2001). The chemical and isotopic compositions of authigenic carbonates provide information concerning the fluids present during precipitation (Naehr et al., 2007; Peckmann et al., 2001). Therefore, authigenic carbonates represent a suitable archive of the palaeohydrological and geological settings present during precipitation.

The present study reports rates of AOM and SR, as well as carbonate mineralogy and isotopy from two adjacent mud extrusions (Mound 11 and 12) located at the subduction zone forearc off the Pacific Costa Rican coast. Sediment and carbonate samples were obtained during a research cruise in 2010. In addition, strontium and carbon isotope data of Mound 11 and 12 carbonates, obtained during previous expeditions, are reported. Microbial turnover rates and stable isotope signatures of carbonate samples retrieved are in accordance with hypothesized fluid discharge processes.

2 Material and methods

2.1 Geological settings and study sites

The Middle American Trench is a large-scale subduction zone with a length of 2750 km located off the southwestern coast of Central America. Offshore Costa Rica, the trench is formed by the eastward subduction of the oceanic Cocos plate beneath the Caribbean plate. A characteristic feature of this trench is the subduction of seamounts and ridges (Ranero and Von Huene, 2000). As these structures are thrusted into and below the continental plate, subduction of material may cause fractures in the upper plate and overlying shelf sediments through which fluids rise towards the surface (Ranero et al., 2000).

Fluid emanation off Costa Rica predominantly occurs at bathymetric elevations, so called mounds, which are ubiquitous and composed of authigenic carbonates, mud

BGD
10, 8159–8201, 2013

extrusions, and hemipelagic sediments (Hensen and Wallmann, 2005). The present study focuses on the two neighboring mounds, Mound 11 and 12 (Figs. 1 and 2), which are situated north-east of the Osa Peninsula (Greinert et al., 2001; Bohrmann et al., 1998) in water depths at ~ 1000 m (Klaucke et al. 2008).

Mound 11 is located at 08°55′20″ N and 84°18′14″ W, including two summits that are ~ 300 m apart, each ~ 250 m in diameter (Klaucke et al., 2008). Previous investigations, including sediment sampling and video survey, showed that the Mound 11 surface consists of fine-grained sediment with mats of sulfur bacteria (Schmidt et al., 2005; Mörz et al., 2005; Mau et al., 2006).

Mound 12 is located about 1 km north of Mound 11 and is characterized by a differing geological morphology, including a solitary summit with a diameter of ~ 800 m (Klaucke et al., 2008). Sediment sampling and video surveys of the sediment surface revealed fine-grained sediment and typical cold-seep features, such as mats of sulfur-oxidizing bacteria, fields of chemosymbiotic vesicomyiid clams and carbonate precipitates (Mau et al., 2006; Linke et al., 2005).

2.2 Sampling and analytical methods

Sediment samples from Mound 11 and 12 were obtained during the research expedition SO206 (June 2010) onboard the German R/V *Sonne*. Stations for sediment recovery on both mounds were situated in water depths of 1000–1010 m (Table 1). Samples were collected with a gravity corer (GC) and a video-guided multicorer (MUC). MUC sampling was performed at locations with microbial mats of filamentous sulfur-oxidizing bacteria visible on the sediment surface, indicating areas of high methane flux (Treude et al., 2003; Torres et al., 2004). In addition, carbonate samples obtained from Mound 12 during the three previous cruises were also used in this study: SO173/4 (September 2003) onboard the R/V *Sonne*, M66/3a (October–November 2005), and M54/3a (September 2002) on board the R/V *Meteor* (Table 1).

BGD
10, 8159–8201, 2013

2.3 Core processing for porewater extraction

The GC obtained at SO206-50 was sectioned into 1 m intervals and cut in half. One half was stored at 4 °C, serving as archive. The other half was used for sediment and porewater sampling. Nine samples were obtained in 30–45 cm intervals over a total length of 300 cm for porewater extraction. From each MUC cast (Mound 11, SO206-39; Mound 12, SO206-44 & 46), one core was assigned for sediment porewater analysis. The three MUCs were sectioned in 1 cm intervals and sampled at 10 depths between core top and bottom.

2.4 Porewater analysis

Porewater was gained from sediments using a pressure filtration system (argon 3–4 bars, 0.2 µm regenerated cellulose filters). Retrieved porewater was analyzed on board for total alkalinity (TA) and total sulfide concentrations. Additional porewater samples were taken for sulfate and chloride concentration measurements on land.

For TA determination, 1 mL of porewater was titrated manually with 0.01 M HCl using a titration vessel after G. Pavlova and a MetromTitrino plus titration unit. A Methyl Red/Methylen Blue solution with the following composition was used as indicator: sodium salt of Methyl Red (37 mg) was mixed with 1.19 mL of 0.1 M NaOH and dissolved in 80 mL Ethanol (96 %) (solution 1). Methylene Blue (10 mg) was dissolved in 10 mL Ethanol (96 %) (solution 2). Both solutions were mixed (80 mL of solution 1 and 4.8 mL of solution 2) to obtain a greenish-brown product. IAPSO standard seawater was used for TA calibration. Hydrogen sulfide concentration measurements were carried out photometrically after Cline (1969). For sulfide calibration Titrisol®-Standard 0.1 N $Na_2S_2O_3$ was used. For sulfate measurements porewater samples were acidified with ultra-purified HNO_3 (65 %) and cooled to 4 °C until further use. Sulfate and chloride concentrations were determined using ionchromatography (METHROM 761) at facilities at GEOMAR, Kiel.

BGD
10, 8159–8201, 2013

2.5 Ex situ microbial turnover rates of methane and sulfate

Immediately after retrieval of the MUC, six replicate polycarbonate push- cores (3 for AOM rates, 3 for SR rates, inner diameter 26 mm, length 25 cm) were sampled from pristine surface sediment of one multicorer core (inner diameter 100 mm). Sediment from gravity corers was sampled with six 5 mL glass tubes, closed with syringe puncheons, dipped in Antifoam®, to enable a better gliding. Open ends of push-cores and glass tubes were closed with rubber stoppers for anoxic incubation. In addition, 10 controls (5 mL each) were sampled from sediment from the same core (GC or MUC) using 5 mL syringes with cut off tips.

2.6 Anaerobic oxidation of methane (AOM)

On board, radioactive methane ($^{14}CH_4$ dissolved in water, 15 µl injection volume, activity 1–2 kBq, specific activity 2.28 GBq mmol^{-1}) was injected into replicate push cores at 1 cm intervals according to the whole-core injection method of Jørgensen (1978). After tracer injection, push cores were incubated at in situ temperature (8 °C) for 24 h in the dark. Subsequently, microbial activity was terminated by sectioning 1 cm intervals of sediment into 50 mL glass vials filled with 25 mL of sodium hydroxide (2.5 % w/w). Vials were closed immediately after sediment transfer and shaken vigorously before storage. Controls were first transferred into sodium hydroxide before addition of radiotracer. At GEOMAR (Kiel), AOM rates were determined after Treude et al. (2005) (gas chromatography, $^{14}CH_4$ combustion, and calculation) and Joye et al. (2004) ($^{14}CO_2$ trapping).

2.7 Sulfate reduction (SR) rates

Sampling, injection, and incubation conditions were identical to that of the AOM samples. The injected radiotracer was radioactive sulfate ($^{35}SO_4^{2-}$ dissolved in water, 6 µL injection volume, activity 200 kBq, specific activity 37 TBq mmol^{-1}). After 24 h, microbial

BGD
10, 8159–8201, 2013

activity was terminated by sectioning 1 cm intervals of sediment into 50 ml plastic centrifuge vials filled with 20 mL zinc acetate (20 % w/w). Controls were first transferred into zinc acetate before addition of radiotracer. SR rates were determined using the cold-chromium distillation method by Kallmeyer et al. (2004).

2.8 Carbonate sampling

Carbonate blocks present in GC and MUC samples that were between 2 and 12 cm in length, were picked with gloves, wrapped in aluminum foil, and subsequently stored at −20 °C. Two bivalve shell fragments found within sediment from SO206-39 (MUC) were sampled accordingly. An overview of carbonate samples taken from GC and MUC cores is provided in Table 2.

2.9 Determination of methane concentrations

Methane was stripped from sediments according to the method of McAullife (1971). Sediment plugs were recovered using a 10 mL clean disposable polypropylene syringe that had the end cut off. The sediment plug was immediately injected in a 30 mL glass vial filled with 10 mL of 10 % aqueous solution of potassium chloride (KCl). The vial was sealed and vigorously shaken to disaggregate the mud and to stop all bacterial activity via KCl poisoning (Bowes and Hornibrook, 2006). The sample was stored upside down, to minimize potential gas exchange with the atmosphere, and allowed to equilibrate with the vial headspace for 48 h. The gas was extracted with a syringe while injecting an equivalent amount of 10 % KCl solution. A blank sample (air equilibrated with 10 % KCl solution) was taken for background corrections. The KCl solution was not acidified so as to avoid production of CO_2 by dissolution of carbonate minerals. The headspace gas was later transferred into either a 10 or 20 mL sterile serum vial, filled (bubble-free) with a pH 1, 10 % KCl solution, by displacement of an equivalent amount of solution. The vials were stored upside down. The methane concentration was determined onboard by **G**as **C**hromatography-**F**lame **I**onization **D**etection (GC-FID) using

BGD
10, 8159–8201, 2013

a Shimadzu GC14A instrument fitted with a Restek Rt® Alumina Bond/KCl capillary column (50 m, 0.53 mm ID) operated at 60 °C. N2 was used as a carrier gas.

2.10 X-ray diffraction of carbonates

Carbonate samples and bivalve shell fragments were dried at 37 °C for 12 hrs and gently cleaned from sediment remains. The top surface from each carbonate piece was scoured away in an area of ~5 × 5 mm. Subsequently; a small cavity was drilled to yield mineral powder. Powder from carbonate samples was analyzed for mineralogy using x-ray diffraction (Philips X-ray diffractometer PW 1710 with monochromatic CoKα) between 2 and 70 2θ (incident angle). The resulting spectra were analyzed with the software XPowder® (XPowder, Spain).

2.11 Isotope analysis of carbonates

From each homogenized carbonate powder sample (see above), an aliquot of 10 mg was separated for carbon δ^{13}C and oxygen δ^{18}O stable isotope analysis. A fraction from this (approximately 1 mg) was dissolved by water-free phosphoric acid at 73 °C in a "Carbo-Kiel" (Thermo Fischer Scientific Inc.) online carbonate preparation line and measured for carbon and oxygen stable isotope ratios with a MAT 253 mass spectrometer (Thermo-Fischer Inc.). The δ^{13}C and δ^{18}O values are reported as ‰ deviations from laboratory standard referred to the V-PDB scale. The standard deviations given were based on replicate analyses (n = 7) of the laboratory standard.

In addition, strontium and carbon isotope data as well as mineralogy of carbonates, sampled at Mound 11 and 12 during previous cruises (SO173/4, M66/3a, and M54/3a), are presented (Table 2). Strontium isotope ratios were determined by **T**hermal **I**onization **M**ass **S**pectrometry (TIMS) after chemical separation by cation exchange chromatography using Sr-specific resin (Eichrom). Presented strontium isotope data are normalized to a ^{87}Sr / ^{86}Sr ratio of 0.710248 for NIST 987 according to McArthur et

BGD
10, 8159–8201, 2013

al. (1998). IAPSO standard seawater was measured as a reference for modern seawater $^{87}Sr/^{86}Sr$. During the present study analytical precision of samples was higher than the external reproducibility of $\pm 1.5 \times 10^{-5}$ (2σ). Only sample SO173 110-1-a (Table 6) showed a lower precision (2.1×10^{-5} 2σ).

2.12 Numerical modeling of measured data

A one-dimensional transport-reaction model similar to previously published approaches (Hensen and Wallmann, 2005; Schmidt et al., 2005; Wallmann et al., 2006) was formulated to simulate the measured pore water profiles of Cl^-, SO_4^{2-}, CH_4, H_2S, TA, and Ca^{2+} and to quantify upward flow velocities, benthic fluxes, as well as rates of AOM and $CaCO_3$ precipitation. The model considered pore water advection and irrigation (mixing), sediment accumulation and molecular diffusion of dissolved species. Organic matter degradation was not simulated, as its rate is assumed to be insignificant compared to methane-related SR and AOM (Karaca et al., 2010; Wallmann et al., 2006).

A time-dependent partial differential equation based on the classical approach for early diagenesis by (Berner, 1980) was used

$$\varphi \cdot \frac{\partial [C]}{\partial t} = \partial \left(\frac{\varphi \cdot D_{\text{sed}} \cdot \frac{\partial [C]}{\partial x}}{\partial x} \right) - \varphi \cdot v \cdot \frac{\partial [C]}{\partial x} + \varphi \cdot R, \quad (2)$$

where $[C]$ is the concentration of dissolved species in pore fluids (mmol L^{-1}), t is the time (yr), x is the sediment depth (cm), φ is the sediment porosity, D_{sed} is the molecular diffusion coefficient in sediments ($cm^2\,yr^{-1}$), v is the vertical advection velocity of pore fluid ($cm\,yr^{-1}$), R represents all reactions considered in the simulated sediment domain.

Assuming steady state compaction, the sediment burial velocity can be expressed as

$$\omega(x) = \frac{(1 - \phi_{\text{bot}}) \cdot \omega_{\text{bot}}}{(1 - \phi(x))}, \quad (3)$$

BGD
10, 8159–8201, 2013

where $\omega(x)$ is the depth-dependent burial velocity, ω_{bot} is the sedimentation rate at the lower boundary ($cm\,a^{-1}$), and ϕ_{bot} is the porosity at the lower boundary. Due to compaction sediment porosity decreases with depth and can be approximated by

$$\phi(x) = \left(\phi_{top} - \phi_{bot}\right) \cdot e^{(-const \cdot x)} + \phi_{bot}, \quad (4)$$

where ϕ_{top} is the porosity at the upper boundary and const is the attenuation coefficient for the decrease of porosity with depth.

The vertical velocity of pore fluid advection through sediments consists of the following components (i) downward burial, (ii) compaction, and (iii) upward fluid advection and can be expressed as

$$v(x) = \frac{\omega_{bot} \cdot \phi_{bot} - v_{top} \cdot \phi_{top}}{\phi(x)}, \quad (5)$$

where $v(x)$ is the depth-dependent fluid velocity and v_{top} is the upward directed fluid velocity at the sediment surface.

Temperature-dependent molecular diffusion coefficients of dissolved Cl^-, SO_4^{2-}, CH_4, HS^-, HCO_3^-, and Ca^{2+} were calculated according to (Boudreau, 1997) and corrected for tortuosity

$$D_{sed}(x) = \frac{D_0(x)}{1 - \ln(\phi(x))^2}, \quad (6)$$

where $D_0(x)$ is the molecular diffusion coefficient in seawater.

Admixing of bottom water into the upper sediment column is a process which is typically observed in seep environments and has been ascribed to various processes such as density-driven formation of convection cells or irrigation through bubble ebullition (Henry et al., 1996; Haeckel et al., 2007). In general, such type of process can be simulated by including a non-local mixing term (Boudreau and Marinelli, 1994; Schmidt et al., 2005):

$$R_{mix}(x) = \alpha(x) \cdot (C(x) - C(0)), \quad (7)$$

BGD
10, 8159–8201, 2013

$$\alpha = \frac{\alpha'}{\left(1 + e^{(x - x_{\mathrm{mix}})/w_{\mathrm{mix}}}\right)}, \tag{8}$$

where α' and $\alpha(x)$ are the pore water mixing coefficient and the depth-dependant pore water mixing coefficient (yr^{-1}), respectively, $(C(x) - C(0)$ is the difference in solute concentration between seawater and any sediment depth, x_{mix} is the depth of the mixing layer in cm, and w_{mix} represents the thickness of the transition layer in cm (proportion of sediment column between mixed and non-mixed area).

Methane is oxidized by sulfate and production of hydrogen sulfide and bicarbonate (AOM)

$$\mathrm{CH_4} + \mathrm{SO_4^{2-}} \rightarrow \mathrm{HCO_3^-} + \mathrm{HS^-} + \mathrm{H_2O}, \tag{9}$$

which was calculated as a second-order rate law

$$R_{\mathrm{AOM}}(x,t) = k_{\mathrm{AOM}} \cdot [\mathrm{SO_4^{2-}}] \cdot [\mathrm{CH_4}], \tag{10}$$

where k_{AOM} is the kinetic constant for the anaerobic oxidation of methane (in $\mathrm{mmol\,cm^{-3}\,yr^{-1}}$).

In order to produce fits to pore water profiles of dissolved hydrogen sulfide, precipitation of iron sulfides is assumed using Equation 11 as suggested by Wallmann et al. (2008):

$$\mathrm{H_2S} + \frac{2}{5}\mathrm{Fe_2O_3} \rightarrow \frac{2}{5}\mathrm{FeS_2} + \frac{1}{5}\mathrm{FeS} + \frac{1}{5}\mathrm{FeO} + \mathrm{H_2O}. \tag{11}$$

The general depth-dependent function of sulfide removal from pore fluid is defined as

$$R_{\mathrm{Sprec}}(x,t) = \frac{[\mathrm{H_2S}]}{K_{\mathrm{SP}} + [\mathrm{H_2S}]} \cdot k_{\mathrm{reS}} \cdot e^{(-\mathrm{remS} - x)}, \tag{12}$$

BGD
10, 8159–8201, 2013

where K_{SP} is the Michaelis-Menten constant for sulfide removal in mmol cm^{-3}, k_{reS} is the kinetic constant for total HS^- removal from pore fluids in mmol cm^{-3} yr^{-1}, and remS is the attenuation coefficient for the decrease in HS^- removal rate with depth in cm^{-1}.

Rates of $CaCO_3$ precipitation were derived by fitting the model curve to the porewater Ca^{2+}-profile waters:

$$R_{Ca}(x,t) = k_{Ca} \cdot (Ca_{meas}(x) - Ca_{mod}(x,t)). \quad (13)$$

An analytical function was fit through the data ($Ca^{2+}_{meas}(x,t)$) so Ca^{2+} concentrations calculated in the model for each depth interval and time step ($Ca^{2+}_{mod}(x,t)$) could be compared and $CaCO_3$ was precipitated until the calculated Ca^{2+} concentrations approached those measured in the investigated sediment cores. Precipitation rates were adjusted by varying the rate constant k_{Ca} (in yr^{-1}). Precipitation of $CaCO_3$ consumes two moles of bicarbonate per mol of Ca^{2+} (Eq. 17), which is considered in the model calculation for TA.

$$Ca^{2+} + 2HCO_3^- \rightarrow CaCO_3 + CO_2 + H_2O. \quad (14)$$

The loss of HCO_3^- during precipitation of $CaCO_3$ was considered for a simplified modelling of TA as well. TA was defined as:

$$TA = HCO_3^- + 2CO_3^{2-} + HS^-, \quad (15)$$

neglecting minor pore water constituents such as $B(OH)_4^-$. In order to provide a meaningful comparison between modelled and measured alkalinity data, measured TH_2S values were subtracted from TA (TH_2S is dominantly HS^- at typical ambient pH values of ~ 8).

At the upper and lower boundary of the model column, constant concentrations of dissolved species were prescribed (Dirichlet boundary conditions). The individual bottom water background concentrations of chemical species were defined as upper

BGD
10, 8159–8201, 2013

boundary conditions (0 cm) for each of the four modeled cores. Chemical species concentrations at the base of the cores served as lower boundary conditions (see Table 3).

Reliable measurements of dissolved methane were not available since most of the dissolved methane is typically lost during core retrieval (e.g. Hensen et al., 2007). Because all modeled cores indicate methane saturation at some depth below the zone of sulfate penetration, methane concentrations at the lower boundary were defined by calculating the (temperature-, pressure- and chlorinity-dependent) solubility with respect to free methane gas (IUPAC, 1987; Tishchenko et al., 2005) for each core separately.

Overall, central finite differences were applied to approximate the spatial derivatives of the partial differential equations (PDEs). The NDSolve object of Mathematica® Version 7.0 (method-of-lines technique) was used to solve the resulting systems of ordinary differential equations (ODEs). The upper and lower boundary conditions as well as other model parameters are summarized in Table 3. Based on the modeling results, depth-integrated rates for AOM, sulfide precipitation, and calcium carbonate precipitation were calculated. In addition, total benthic fluxes of the 6 dissolved species were derived.

3 Results

3.1 Porewater chemistry and microbial turnover rates

Biogeochemical profiles obtained at Mound 11, stations SO206-39 (MUC) and SO206-50 (GC), respectively (Fig. 3), revealed considerable differences regarding the vertical position of the sulfate-methane transition zone (SMT) and the location of peak microbial turnover rates of methane and sulfate. The sediment core from SO206-39 showed a strong decline of sulfate from a surface concentration of 27.4 mmol SO_4^{2-} L^{-1} to < 0.5 mmol L^{-1} within the first 6 cm below seafloor (cmbsf). Methane concentration increased from 2 mmol CH_4 L^{-1} at 21 cm b.s.f. to 17.9 mmol CH_4 L^{-1} at 7.5 cm b.s.f. Towards the surface, values further declined to 0.6 mmol CH_4 L^{-1}. The SMT was located

BGD
10, 8159–8201, 2013

at ~5 cm b.s.f. Sulfate concentration at station SO206-50 (GC) decreased from a surface concentration of 27.5 mmol SO_4^{2-} L^{-1} to < 0.5 mmol SO_4^{2-} L^{-1} at 150.5 cm b.s.f. Methane declined from 5.1 mmol CH_4 L^{-1} at the bottom of the core (290 cm b.s.f.) to 1.9 mmol CH_4 L^{-1} at 210 cm b.s.f. At a sediment depth of 190 cm b.s.f. methane concentration steeply increased to 20.9 mmol CH_4 L^{-1}, followed by a sharp decline to a surface concentration of 0.06 mmol CH_4 L^{-1}. The SMT at station SO206-50 was located at ~ 125 cm b.s.f., i.e., considerably deeper compared to SO206-39.

At Mound 11, AOM and SR rates from SO206-39 showed peak values of 4.4 µmol CH_4 cm^{-3} d^{-1} and 8.1 µmol SO_4^{2-} cm^{-3} d^{-1}, respectively, between 2 and 5 cm b.s.f. Corresponding integrated average areal rates (0–10 cm) were 140.71 (±40.84 SD, n = 3) mmol CH_4 m^{-2} d^{-1} for AOM and 117.25 (±82.06 SD, n = 3) mmol SO_4^{2-} m^{-2} d^{-1} for SR (Table 4). At SO206-50, maximum rates for AOM and SR reached 0.01 µmol CH_4 cm^{-3} d^{-1} and 0.017 µmol SO_4^{2-} cm^{-3} d^{-1}, respectively, at 65 cm b.s.f. Corresponding areal rates, integrated over the sampled core length (290 cm) yielded average values of 4.76 (±2.21 SD, n = 3) mmol CH_4 m^{-2} d^{-1} for AOM and 45.48 (±53.67 SD, n = 3) mmol SO_4^{2-} m^{-2} d^{-1} for SR, respectively. Despite the differences in AOM and SR rates of stations SO206-50 and SO206-39, maximum sulfide (2.3 and 4.4 mmol L^{-1}) and total alkalinity (2.1 and 4.2 mEq) levels were in the same order of magnitude in both cores.

At Mound 12, the sulfate and methane concentration profiles differed between the two stations SO206-44 (MUC) and SO206-46 (MUC) (Fig. 4). In SO206-44 sediment, sulfate decreased gradually from surface concentrations of 28.4 to 4.2 mmol SO_4^{2-} L^{-1} between 5–7 cm b.s.f. Below this depth, sulfate concentration declined to 1.4 mmol SO_4^{2-} L^{-1} at the core bottom (13 cmbsf). Methane concentrations in SO206-44 sediment varied considerably over the entire core length of 20 cm. At the surface, methane concentration was 3.5 mmol CH_4 L^{-1}, followed by an increase to ~ 14 mmol CH_4 L^{-1} between 2.5 to 6.5 cm b.s.f. Below this depth, methane concentration varied between 1 and 12 mmol CH_4 L^{-1}. Due to the presence of massive

BGD
10, 8159–8201, 2013

carbonate layers in the sediment, core liner penetration at SO206-46 was limited to 12 – 15 cmbsf. Sulfate declined from surface concentrations of 28.3 mmol SO_4^{2-} L^{-1} to 11.5 mmol SO_4^{2-} L^{-1} at 9 cm b.s.f. Methane increased from 1.3 to 19.1 mmol CH_4 L^{-1} between 11 and 9 cm b.s.f., declining steeply to < 0.2 mmol CH_4 L^{-1} towards the sediment surface.

Highest rates for AOM and SR at Mound 12 were measured between 2 and 5 cm b.s.f. at both stations. At station SO206-44, peak values of 0.58 µmol CH_4 cm^{-3} d^{-1} and 0.52 µmol SO_4^{2-} cm^{-3} d^{-1}, respectively, were measured. Integrated average areal rates of the top 10 cm yielded 22.37 (±0.85 SD, n = 3) mmol CH_4 m^{-2} d^{-1} and 23.99 (±5.79 SD, n = 3) mmol SO_4^{2-} m^{-2} d^{-1} for AOM and SR, respectively (Table 4). At station SO206-46, microbial rates were slightly higher, reaching maximum values of 0.65 µmol CH_4 cm^{-3} d^{-1} (AOM) and 2.30 (SR). Corresponding average areal rates were 10.68 (±3.53 SD, n = 3) for AOM and 64.97 (±6.79 SD, n = 3) for SR, respectively.

In accordance with peak AOM and SR, highest concentrations of total alkalinity (~ 13.5 and 6.4 mEq for Mound 11 and 12, respectively) and sulfide (2.2 to 4.4 and 8.5 to 10.0 µmol L^{-1} for Mound 11 and 12, respectively) were located within the SMT at both mounds (Fig. 3 and 4). Only station SO206-44 at Mound 12 showed increasing total alkalinity below the SMT (from 28.8 to 33.1 mEq). At Mound 11, stations SO206-39 and SO206-50 revealed a sharp peak (17.9 and 20.9 mmol L^{-1}, respectively) of the methane profiles at the lower proximity of the SMT zone. In the GC 50 core, the CH_4 peak coincided with a large block of gas hydrate located at ~ 12 cm b.s.f. Therefore, we assume that gas hydrate dissociation during core retrieval caused the local methane peak in the sediment.

3.2 Numerical modeling results

The rates for advective fluid flow, AOM, and calcium carbonate precipitation were determined by fitting the model to the porewater data. Parameter values and boundary

BGD
10, 8159–8201, 2013

conditions used for simulations (Table 3) yielded good fits to the measured porewater profiles (see supplementary information, Fig. 1S–4S). Considerable deviations between model results and porewater data occurred only for methane and hydrogen sulfide profiles, as measured concentrations were lower than simulated values. This discrepancy is caused by the loss of methane and hydrogen sulfide, respectively, due to outgassing during core retrieval and has been reported before (e.g. Karaca et al., 2010; Hensen et al., 2007).

The depth-integrated AOM rates differed considerably between the two cores obtained at Mound 11 (SO206-39 (MUC) and SO206-50 (GC)) (Table 4). For station SO206-39 an AOM rate of 188.3 mmol CH_4 m^{-2} d^{-1} (integrated from 0 to 100 cm sediment depth) was calculated. In contrast, at station SO206-50 the modeled AOM rate (integrated from 0 to 500 cm sediment depth) was one order of magnitude lower (15.9 mmol CH_4 m^{-2} d^{-1}). The two stations at Mound 12 (SO206-44 (MUC), SO206-46 (MUC)) showed modeled AOM rates (each integrated from 0 to 100 cm sediment depth) of 127.3 and 161.6 mmol CH_4 m^{-2} d^{-1}, respectively. Between stations SO206-39 and SO206-50 (Mound 11) depth-integrated calcium carbonate precipitation rates varied between 1.3 and 6.1 mmol $CaCO_3$ m^{-2} d^{-1}, respectively, while the two stations from Mound 12 showed higher values of 13.3 (SO206-44) and 15.3 mmol Ca^{2+} m^{-2} d^{-1} (SO206-46).

According to model results, considerable differences of sediment- water column total fluxes of the 6 dissolved chemical species occurred between the four stations. Due to the 1:1 stoichiometry of methane and sulfate consumption during AOM, the total in-flux of sulfate from the water column into the sediment was in accordance with the depth-integrated AOM rates at the four stations with highest sulfate fluxes at station SO206-39 (Mound 11) and SO206-46 (Mound 12) of 188.9 and 161.6 mmol SO_4^{2-} m^{-2} d^{-1}, respectively. The calculated methane flux yielded negative values for all stations, indicating an upward directed flux inside the sediment. The two stations at Mound 11 showed contrasting values for methane flux, ranging from 675.3 (SO206-39) to 3.3 mmol CH_4 m^{-2} d^{-1} (SO206-50). Also the two stations at Mound 12 largely differed

BGD
10, 8159–8201, 2013

in upward methane flux, showing values of 124.5 and 14.9 mmol CH_4 m^{-2} d^{-1}, respectively. Modeled total flux of carbon, taking into account methane advection rate, AOM rate and carbonate precipitation rate, showed carbon export from the sediment into the water column at both mounds. In accordance to fluid flow and AOM rate, highest carbon flux was found at station SO206-39 (Mound 11, 237.7 mmol C m^{-2} d^{-1}), while the corresponding flux rate at the neighboring station SO206-50 was two orders of magnitude lower (3.7 mmol C m^{-2} d^{-1}). At the two stations at Mound 12 total upward carbon flux ranged between 150.5 (SO206-44) and 232.1 mmol C m^{-2} d^{-1} (SO206-46). Modeled flux rates of calcium showed a downward flux into the sediment of 104.5 and 13.5 mmol Ca^{2+} m^{-2} d^{-1} at stations SO206-39 (Mound 11) and SO1206-46 (Mound 12), respectively. In contrast, stations SO206-50 (Mound 11) and SO206-44 (Mound 12) were characterized by upward calcium fluxes of 4.0 and 3.3 mmol Ca^{2+} m^{-2} d^{-1}, respectively.

3.3 Carbonate mineralogy and isotopic composition

The results for mineralogy and isotopic composition of oxygen and carbon of sampled carbonate concretions are compiled in Tables 5 and 6. XRD analyses confirmed generally high carbonate content of the concretions, ranging from 10 % to 82 % and 77 % to > 98 % at Mound 11 and 12, respectively. XRD spectra further showed that the carbonate samples mainly consisted of Aragonite and Mg-calcite, generally accounting for >95 and 51 % of the carbonate mass, respectively. Mg-free calcite was also present, contributing between 23 % and 30 % to the carbonate mass. At Mound 11, also ferric dolomite and kutnahorite appeared in samples collected from sediment depths > 10 cm b.s.f. However, relative contribution to the carbonate mineral phases did not exceed 8 %. Bivalve shell fragments, most likely belonging to the vesicomyiid family, from Mound 11 differed from authigenic carbonate samples, consisting of aragonite.

Carbonate samples from Mound 11 were characterized by $\delta^{13}C$ values ranging from −30 ‰ to −14 ‰ (Table 4, Table 6, Fig. 5). Corresponding $\delta^{18}O$ values varied between

BGD
10, 8159–8201, 2013

4.7 ‰ and 6.2 ‰ (±0.04 SD). The two Mound 11 carbonate samples from M54 had aragonite contents of 10 % and 70 %, respectively. In addition, the carbonate dominated leachates (2.25 N HNO_3) of both showed $^{87}Sr/^{86}Sr$ ratios (0.708829 and 0.709049) (Table 6), which were considerably lower than for modern seawater.

The carbon and oxygen isotopic signatures of carbonate samples obtained from Mound 12 were in general more negative. Values for $\delta^{13}C$ ranged from −49 ‰ and −39 ‰, $\delta^{18}O$ ranged between 4.1 and 4.5 ‰. Isotopic signatures of the two bivalve shell fragments deviated from the authigenic carbonate samples with $\delta^{18}O$ being lower (3.5–4.0 ‰) and $\delta^{13}C$ values being considerably higher (−9.6–6.9 ‰). In contrast to Mound 11, the carbonate samples collected from Mound 12 generally showed higher $^{87}Sr/^{86}Sr$ ratios (0.709088 to 0.709167), ranging close to the value for modern seawater (0.709176) (Table 6). Analysis uncertainties of $^{87}Sr/^{86}Sr$ ratios were generally $< 2\sigma 1.5 \times 10^{-5}$, only sample SO173 110-1a showed a 2σ of 2.1×10^{-5}.

4 Discussion

In the present study, considerable differences of AOM and SR as well as $\delta^{18}O$, $\delta^{13}C$, and $^{87}Sr/^{86}Sr$ isotopic signatures of carbonates from surface sediment samples of the two neighboring mounds are indicative for different fluid regimes underlying them. In the following sections differences in microbial activity and carbonate isotopic signatures between Mound 11 and 12 will be discussed.

4.1 Microbial activity

Measured areal AOM and SR rates obtained from Mound 11 were up to one order of magnitude higher compared to Mound 12, and were in the same order of rates reported for high-advective cold-seep systems such as Hydrate Ridge (Treude et al., 2003) and Håkon Mosby Mud Volcano (Niemann et al., 2006) (Table 4). To our knowledge, areal measured AOM rates of Mound 11 (SO206-39) exceed highest values published for

BGD
10, 8159–8201, 2013

marine cold-seep locations so far (e.g. Treude et al., 2003; Joye et al., 2004; Krüger et al., 2005). However, AOM and SR rates at the Mound 11 station SO206-50 were considerably lower than at SO206-39, illustrating the strong spatial heterogeneity in fluid flow, often encountered at seep locations.

The observed difference in AOM and SR rates between the two mounds might be due to different advective transport velocities of methane charged fluid. This hypothesis is supported by previous reactive-transport modeling (Mound 11) and benthic flux chamber experiments (Mound 12) (Karaca et al., 2010; Linke et al., 2005). According to these studies, maximum fluid flow at Mound 11 may be as high as 200 cm yr^{-1} at the center of the seep (within microbial mat patches), while only approximately 10 cm yr^{-1} was calculated for Mound 12. Based on the porewater data of the used cores, the applied modeling approach of the present study supported previous measurements and estimates of fluid flow velocities at Mound 11 and 12, indicating advective transport being 3 to 7 times faster at Mound 11.

The numerical transport-reaction model for Mound 11 (MUC 39) showed a best fit using a fluid velocity of 50 cm a^{-1}. The modeled depth-integrated areal AOM ratio was in good agreement to the data, yielding an areal AOM rate in the same order of magnitude as the measured one. Thus, comparison of measured and modeled depth-integrated AOM rates at Mound 11 showed that the modeling approach was suitable to describe the methane-related biogeochemical processes.

For stations at Mound 12 best-fit model results were obtained using fluid flow velocities of 8 (station SO206-44) and 15 cm a^{-1} (station SO206-46), supporting previous calculations of Linke et al. (2005) (16.11 cm a^{-1}) and Karaca et al. (2010) (9.64 cm a^{-1}). In contrast to Mound 11, measured and modeled areal AOM rates differed considerably for Mound 12. Here measured rates for both cores (SO206-44, SO206-46) were one order of magnitude lower as predicted by the model. Modeling was carried out using porewater data, obtained from the same multi corer sampling, but not directly from the cores used for rate measurements. Therefore it seems plausible that variations of

BGD
10, 8159–8201, 2013

AOM activity between individual MUC cores were causative for observed differences between measured and modeled areal AOM rates.

Previous studies of seep sites at Hydrate Ridge showed considerable lateral sediment heterogeneity regarding AOM activity (Treude et al., 2003), which can also be assumed for the region off Costa Rica (Hensen et al., 2004; Schmidt et al., 2005; Linke et al., 2005). However, spatial heterogeneity of AOM activity is not accounted for in the used model approach, as it assumed that concentrations and consequently reaction rates only vary with sediment depth. Therefore, the deviation of measurement- and model-based AOM rates does not necessarily indicate that model accuracy was insufficient to describe the methane related biogeochemical processes at Mound 12, but rather illustrates the spatial heterogeneity of sedimentary AOM activity.

It should be mentioned that the here observed differences in measured AOM and SR rates of one order of magnitude in surface sediments covered by thick sulfur bacteria mats illustrates the wide range of methane turnover that can be connected with this type of chemosynthetic habitat. Sulfur bacteria are capable of oxidizing sulfide (Jørgensen and Nelson, 2004), and are typically present at localities of high anaerobic methane turnover (Treude et al., 2003). However, the variability of AOM rates underneath sulfur bacteria mats observed in our study, calls for caution with respect to extrapolations of methane turnover rates based solely on visual seafloor observations.

4.2 Carbonate isotope systematic

The higher δ^{18}O values of carbonates from Mound 11 indicate that this location might be under considerable influence of a deep-source fluid, supporting previous investigations (Han et al., 2004; Hensen et al., 2004; Mavromatis et al. 2012). In contrast, lower δ^{18}O values of Mound 12 carbonates suggest extended mixing of deep-source fluid with oceanic bottom water, also postulated by Mavromatis et al. (2012).

While the observed microbial turnover rates of methane indicate differences in fluid flux and corresponding methane supply, the discrepancy of δ^{18}O and δ^{13}C isotopic signatures of carbonate suggest a different origin of fluids at Mound 11 and 12.

BGD
10, 8159–8201, 2013

Carbonates of the two mounds were mainly composed of Mg-calcite that was strongly depleted in ^{13}C. Mound 11 showed $\delta^{13}C$ values between −21 and −30 ‰, while $\delta^{13}C$ values ranged between −45 and −49 ‰ at Mound 12. Corresponding $\delta^{18}O$ values ranged between 4.7 – 6.2 ‰ at Mound 11 and between 4.1–4.5 ‰ at Mound 12, respectively. These results confirmed previous analyses of samples from the study area (Han et al., 2004). Depletion of the heavier ^{13}C and enrichment of heavier ^{18}O isotope in carbonates is a consequence of a kinetic carbon isotope fractionation during AOM (Aloisi et al., 2002). Hence, the isotopic signature of carbonate concretions, sampled at the two mounds, reflect fluid characteristics present during precipitation. According to Hensen et al. (2004), the observed positive $\delta^{18}O$ values of carbonates from the study area are the result of clay-mineral dehydration at temperatures between 85 and 130 °C in ∼ 12 km depth and subsequent upward fluid transport. Thus, the observed difference in ^{18}O enrichment of carbonates from Mound 11 and 12 might be the result of different admixing of deep source fluid with bottom water. In comparison, carbonate concretions at Mound 11 were less depleted in $\delta^{13}C$, suggesting methane of thermogenic origin predominantly present during concretion formation (Schmidt et al., 2005). In contrast, methane of biogenic origin from a shallower source might have been causative for strongly depleted $\delta^{13}C$ in Mound 12 carbonates (Hensen and Wallmann, 2005).

Han et al. (2004) identified five types of authigenic carbonate associated to fluid vent locations at the Costa Rica margin, based on morphological, petrographic, and stable isotope criteria (referred to the PDB scale): chemoherm carbonates, seepage-associated concretions, gas hydrate-associated concretions, as well as calcareous and dolomitic concretions. Regarding the isotopic composition, carbonate samples obtained for Mound 11 and 12 during the SO206 cruise can visually be divided into two groups (Fig. 5). Group 1 was comprised of Mound 11 carbonates samples, while group 2 included samples from Mound 12. Carbonates from group 1 were characterized by $\delta^{18}O$ values between 5.6 to 6.7 ‰. Corresponding $\delta^{13}C$ values ranged from −21 to −29 ‰. According to the carbonate classification mentioned above, group 1 carbonate-isotope composition is indicative for gas hydrate-associated concretions

BGD
10, 8159–8201, 2013

(δ^{18}O 5.2–6.8 ‰, δ^{13}C −18.6–−29.8 ‰) (Han et al. 2004). This type of carbonate is characterized by layered high Mg-calcite and aragonite precipitated into spaces, previously occupied by gas hydrates before dissociation (Bohrmann et al., 2002; Suess, 2002). The carbonates from group 2 had a lower δ^{18}O signature (4.1–4.5 ‰), while depletion of ^{13}C was stronger compared to group 1 (−39—49 ‰). According to Han et al. (2004), carbonates of group 2 showed an isotopic combination typical for seepage-associated concretions (δ^{18}O 4.3–5.4 ‰, δ^{13}C −44.6—53.0 ‰). This type of carbonate occurs at or near the seafloor, forming small, individual carbonate blocks, concretions and crusts of high Mg- calcite. Bivalve shell material from Mound 11 was mainly composed of aragonite and organic components. Corresponding values of δ^{13}C showed an isotopic signature considerably higher compared to the carbonates (−6.9 and −9.7 ‰), indicating shell formation in seawater with atmospheric CO_2 as a carbon source (Emrich et al., 1970).

The strontium and carbon isotope ratios, in combination with the mineralogy of carbonates, obtained during previous cruises (Table 5, Fig. 6), suggested that the difference in δ^{13}C and ^{87}Sr/^{86}Sr signature between the two mounds was primarily caused by mixing of two end members; one being advective fluid, the other one being bottom water. Considering that Mound 12 carbonates samples were comprised > 95 % of Aragonite, while Mound 11 sample M54/3a GC 155B contained only about 70 % Aragonite, it seems plausible that isotopic signature differences might be influenced by carbonate mineral content of the samples. However, comparing the two carbonate samples obtained at Mound 11, evidently the heavy carbon isotope signature is maintained, while the aragonite contents vary between 10 and 70 %. Therefore, we assumed that fluid-bottom water mixing is not causative for differences in carbon isotope signatures at the two mounds. The ^{87}Sr/^{86}Sr ratios of Mound 11 and 12 carbonates appear to depend on the carbonate content of individual samples, as high contents of aragonite of Mound 12 carbonates are accompanied by ^{87}Sr/^{86}Sr ratios close to seawater. In contrast, Mound 11 carbonate samples with lower aragonite content showed lower ^{87}Sr/^{86}Sr ratios, compared to Mound 12 carbonates. However, considering the

BGD
10, 8159–8201, 2013

differing fluid regimes at the two mounds, it seems plausible that the observed differences in $^{87}Sr/^{86}Sr$ ratios are not primarily caused by the carbonate contents, but by different $^{87}Sr/^{86}Sr$ characteristics of deep-source fluid and bottom water. Consequently, we assumed that fluid-bottom water mixing is not causative for differences in strontium and carbon isotope signatures between the two mounds, indicating different fluid and methane sources at the two mounds. The combination of a rather high carbon isotopic signal (−15.6 to −14.2 ‰) and $^{87}Sr/^{86}Sr$ considerably lower than modern seawater at Mound 11 indeed indicate independently that authigenic carbonate precipitation occurred under considerable influence of deep-source fluid charged with thermogenic methane. In contrast, $^{87}Sr/^{86}Sr$ of carbonates at Mound 12 were similar or only slightly lower than seawater, suggesting less strong advection of deep-source fluid compared to Mound 11. The observed lower carbon isotopic signature at Mound 12 also indicates a rather shallow biogenic source of methane. The present study therefore supports previous investigations by Hensen et al. (2004) and Mavromatis et al. (2012), who also postulated a thermogenic methane source at Mound 11, while Mound 12 was suggested to be dominated by a biogenic methane source.

According to sediment petrographic interpretation, dating of volcanoclastic layers and U/Th dating of carbonates from the two locations (Kutterolf et al., 2008), Mound 11 was considered as currently active, meaning that it is expelling fluids and potentially mud onto the surrounding seafloor since ≥ 15 ka. In contrast, pelagic surface sediments (131 cm thickness) at Mound 12 indicated that vertical mud transport is currently inactive and has been since at least 5 ka (Kutterolf et al., 2008). The results of the present study together with previous work by Linke et al. (2005) clearly demonstrated recent methane-related microbial activity at both mounds. Consequently, also Mound 12 has to be considered as a site of active fluid venting, delivering sufficient methane to support related microbial activity. However, it is possible that fluid and methane migration at mound 12 is heterogeneous and therefore sampling of surface sediments could recover either pelagic or seep sediments, depending on where sampling instruments were deployed. During video surveys of Mound 12 surface sediments, we discovered

BGD
10, 8159–8201, 2013

both areas displaying chemosynthetic communities as well as areas devoid of such, which indicates heterogeneous fluid migration.

As both mounds are situated on the same fault zone, ascending fluids may originate from the same source (Mavromatis et al. 2012). Due to past or on-going tectonic processes, the fluid pathway of Mound 12 might have been compromised, reducing deep source fluid advection at this location. The slightly lighter $\delta^{18}O$ values of Mound 12 carbonates suggest that fluids at this location represent a mixture of deep source fluid with bottom water. In contrast, carbonate $\delta^{13}C$ values indicated that fluids at Mound 11 are primarily charged with deep source thermogenic methane.

5 Summary

Methane charged fluid advection is causative for high microbial activity in surface sediments of the two neighboring mounds, Mound 11 and 12, located at the pacific continental margin off Costa Rica. Anaerobic oxidations of methane (AOM) and sulfate reduction (SR) rates determined ex situ in surface sediments were one order of magnitude higher at Mound 11 compared to Mound 12. Differences in carbonate stable isotope composition and $^{87}Sr/^{86}Sr$ signatures of the two mounds indicated that ascending fluid at Mound 11 originated from a deep source transporting primarily thermogenic methane. In contrast, advecting fluids at Mound 12 were primarily charged with biogenic methane from a shallower source. Our study demonstrated that direct measurements of microbial AOM and SR activity, in combination with numerical modeling and carbonate archives analysis, provides a suitable ground truthing tool to support geophysical measurements in order to constrain spatial and temporal variations of methane charged fluid flow at the Costa Rica continental margin.

BGD
10, 8159–8201, 2013

Supplementary material related to this article is available online at: http://www.biogeosciences-discuss.net/10/8159/2013/bgd-10-8159-2013-supplement.pdf.

Acknowledgements. Funding for the present study was provided by the SFB-574: "Volatiles and Fluids in Subduction Zones" and "The Future Ocean" Cluster of Excellence funded by the German Research Foundation (DFG). We thank the captains and the crew of R/V *Sonne*, and R/V *Meteor* and all staff members who supported work onboard. We would like to acknowledge our colleagues A. Bleyer, B. Domeyer, R. Ebbinghaus, R. Surberg, E. Corrales-Cordero, and E. Piñero for porewater sampling and chemical analyses at sea and in land-based laboratories. J. Hommer, K. Kretschmer and J. Farkas are thanked for radiotracer analysis. We also thank A. Kolevica, L. Haxhiaj, for isotope measurements. J. Heinze, and N. Augustin are thanked for carbonate mineralogy analysis. We also thank I. Klaucke and R. W. Weinrebe for providing bathymetric data. K. Lindhorst is thanked for the generation of bathymetric maps.

The service charges for this open access publication have been covered by a Research Centre of the Helmholtz Association.

References

Aloisi, G., Bouloubassi, I., Heijs, S. K., Pancost, R. D., Pierre, C., Damste, J. S. S., Gottschal, J. C., Forney, L. J., and Rouchy, J.: CH_4-consuming microorganisms and the formation of carbonate crusts at cold seeps, Methods, 203, 195–203 2002.

Barnes, R. O. and Goldberg, E. D.: Methane Production and Consumption in Anoxic Marine-Sediments, Geology, 4, 297–300, 1976.

Berner, R. A.: Early Diagenesis – A Theoretical Approach, Princeton University Press, Princeton, NJ, 1980.

Boetius, A., Ravenschlag, K., Schubert, C. J., Rickert, D., Widdel, F., Gieseke, A., Amann, R., Jorgensen, B. B., Witte, U., and Pfannkuche, O.: A marine microbial consortium apparently mediating anaerobic oxidation of methane, Nature, 407, 623–626, 2000.

Bohrmann, G., Greinert, J., Suess, E., and Torres, M.: Authigenic carbonates from the Cascadia subduction zone and their relation to gas hydrate stability, Geology, 26, 647–650, doi:10.1130/0091-7613(1998)026<0647:ACFTCS>2.3.CO;2, 1998b.
Bohrmann, G., Heeschen, K., Jung, C., Weinrebe, W., Baranov, B., Cailleau, B., Heath, R., Hühnerbach, V., Hort, M., Masson, D., and Trummer, I.: Widespread fluid expulsion along the seafloor of the Costa Rica convergent margin, Terra Nova, 14, 69–79, 2002.
Borowski, W.: Global and local variations of interstitial sulfate gradients in deep-water, continental margin sediments: Sensitivity to underlying methane and gas hydrates, Mar. Geol., 159, 131–154, doi:10.1016/S0025-3227(99)00004-3, 1999.
Boudreau, B. P.: Diagenetic Models and their Implementation: Modelling Transport and Reactions in Aquatic Sediments, Springer Verlag, Berlin, 1997.
Boudreau, B. P. and Marinelli, R. L.: A modelling study of discontinuous biological irrigation, J. Mar. Res., 52, 947–968, 1994.
Bowes, H. L. and Hornibrook, E. R. C.: Emission of highly 13C-depleted methane from an upland blanket mire, Geophys. Res. Lett., 33, 1–4, 2006.
Cline, J. D.: Spectrophotometric determination of hydrogen sulfide in natural waters, Limnol. Oceanogr., 14, 454–458, 1969.
Ellam, R. M. and Hawkesworth, C. J.: Elemental and isotopic variations in subduction related basalts: evidence for a three component model, Cont. Mineral. Petrol., 98, 72–80, doi:10.1007/BF00371911, 1988.
Greinert, J., Bohrmann, G., and Suess, E.: Gas Hydrate-associated carbonates and methane-venting at Hydrate Ridge?: Classification, distribution, and origin of authigenic lithologies, in: Geophysical Monograph Series, vol. 124, edited by: Paull, C. K. and Dillon, W. P., 99–113, AGU, Washington, DC, 2001.
Haeckel, M., Boudreau, B. P., and Wallmann, K.: Bubble-induced porewater mixing: A 3-D model for deep porewater irrigation, Geochim. Cosmochim. Ac., 71, 5135–5154, doi:10.1016/j.gca.2007.08.011, 2007.
Han, X., Suess, E., Sahling, H., and Wallmann, K.: Fluid venting activity on the Costa Rica margin: new results from authigenic carbonates, Int. J. Earth Sci., 596–611, doi:10.1007/s00531-004-0402-y, 2004.
Henry, P., Le Pichon, X., Lallemant, S., Lance, S., Martin, J. B., Foucher, J. P., Fiala-Médioni, A., Rostek, F., Guilhaumou, N., Pranal, V., and Castrec, M.: Fluid flow in and around a mud

BGD
10, 8159–8201, 2013

volcano field seaward of the Barbados accretionary wedge: Results from Manon cruise, J. Geophys. Res., 101, 297–323, 1996.
Hensen, C. and Wallmann, K.: Methane formation at Costa Rica continental margin – constraints for gas hydrate inventories and cross-décollement fluid flow, Earth Planet. Sci. Lett., 236, 41–60, doi:10.1016/j.epsl.2005.06.007, 2005.
Hensen, C., Wallmann, K., Schmidt, M., Ranero, C. R., and Suess, E.: Fluid expulsion related to mud extrusion off Costa Rica – A window to the subducting slab, Geology, 32, 201–204, 2004.
Hensen, C., Nuzzo, M., Hornibrook, E., Pinheiro, L., Bock, B., Magalhaes, V., and Bruckmann, W.: Sources of mud volcano fluids in the Gulf of Cadiz—indications for hydrothermal imprint, Geochim. Cosmochim. Ac., 71, 1232–1248, doi:10.1016/j.gca.2006.11.022, 2007.
IUPAC: Methane (IUPAC Solubility Data), edited by: Clever, H. L. and Young, C. L., Pergamon., 1987.
Jørgensen, B. B.: A comparison of methods for the quantification of bacterial sulphate reduction in coastal marine sediments: I. Measurements with radiotracer techniques, Geomicrobiol. J., 1, 11–27, 1978.
Jørgensen, B. B. and Nelson, D. C.: Sulfide oxidation in marine sediments: Geochemistry meets microbiology, Geol. Soc. Am. Special Paper, 379, 63–81, 2004.
Joye, S. B., Boetius, A., Orcutt, B. N., Montoya, J. P., Schulz, H. N., Erickson, M. J., and Logo, S. K.: The anaerobic oxidation of methane and sulfate reduction in sediments from Gulf of Mexico cold seeps, Chem. Geol., 205, 219–238, doi:10.1016/j.chemgeo.2003.12.019, 2004.
Judd, A. G., Hovland, M., Dimitrov, L. I., Gil, S. G., and Jukes, V.: The geological methane budget at Continental Margins and its influence on climate change, Geofluids, 2, 109–126, 2002.
Kallmeyer, J., Ferdelman, T. G., Weber, A., Fossing, H., and Jørgensen, B. B.: A cold chromium distillation procedure for radiolabeled sulfide applied to sulfate reduction measurements, Limnol. Oceanogr.-Methods, 2, 171–180, 2004.
Karaca, D., Hensen, C., and Wallmann, K.: Controls on authigenic carbonate precipitation at cold seeps along the convergent margin off Costa Rica, Geochem. Geophy. Geosy., 11, 1–19, doi:10.1029/2010GC003062, 2010.
Krüger, M., Treude, T., Wolters, H., Nauhaus, K., and Boetius, A.: Microbial methane turnover in different marine habitats, Palaeogeogr. Palaeocl., 227, 6–17, doi:10.1016/j.palaeo.2005.04.031, 2005.

BGD
10, 8159–8201, 2013

Kutterolf, S., Liebetrau, V., Mörz, T., Freundt, A., Hammerich, T., and Garbe-Schönberg, D.: Lifetime and cyclicity of fluid venting at forearc mound structures determined by tephrostratigraphy and radiometric dating of authigenic carbonates, Geology, 36, 707, doi:10.1130/G24806A.1, 2008.

Linke, P., Wallmann, K., Suess, E., Hensen, C., and Rehder, G.: In situ benthic fluxes from an intermittently active mud volcano at the Costa Rica convergent margin, Earth Planet. Sci. Lett., 235, 79–95, doi:10.1016/j.epsl.2005.03.009, 2005.

Manning, C.: The chemistry of subduction-zone fluids, Earth Planet. Sci. Lett., 223, 1–16, doi:10.1016/j.epsl.2004.04.030, 2004.

Martens, C. S. and Berner, R. A.: Methane Production in the Interstitial Waters of Sulfate-Depleted Marine Sediments i I, Science, 185, 1167–1169, 1974.

Mau, S., Sahling, H., Rehder, G., Suess, E., Linke, P., and Soeding, E.: Estimates of methane output from mud extrusions at the erosive convergent margin off Costa Rica, Mar. Geol., 225, 129–144, 2006.

Mavromatis, V., Botz, R., Schmidt, M., Liebetrau, V., and Hensen, C.: Formation of carbonate concretions in surface sediments of two mud mounds, offshore Costa Rica – a stable isotope study, Int. J. Earth Sci., doi:10.1007/s00531-012-0843-7, 2012.

McArthur, J. M., Thirlwall, M. F., Engkilde, M., Zinsmeister, W. J., and Howarth, R. J.: Strontium isotope profiles across K/T boundary sequences in Denmark and Antarctica, Earth Planet. Sci. Lett., 160, 179–192, doi:10.1016/S0012-821X(98)00058-2, 1998.

McAullife, C.: GC determination of solutes by multiple phase equilibration, Chem. Technol., 1, 46–51, 1971.

Mörz, T., Fekete, N., Kopf, A. J., Brueckmann, W., Kreiter, S., Huehnerbach, V., Masson, D. G., Hepp, D. A., Schmidt, M., Kutterolf, S., Sahling, H., Abegg, F., Spiess, V., Suess, E., and Ranero, C. R.: Styles and productivity of mud diapirism along the Middle American Margin, Part II, Mound Culebra and Mounds 11 and 12, in Mud volcanoes, geodynamics and seismicity, edited by: Martinelli, G. and Panahi, B., 49–76, Springer, Dordrecht, the Netherlands, 2005.

Naehr, T. H., Eichhubl, P., Orphan, V. J., Hovland, M., Paull, C. K., Ussler, W., Lorenson, T. D., and Greene, H. G.: Authigenic carbonate formation at hydrocarbon seeps in continental margin sediments: A comparative study, Deep-Sea Res. Pt. II, 54, 1268–1291, 2007.

Niemann, H., Lösekann, T., De Beer, D., Elvert, M., Nadalig, T., Knittel, K., Amann, R., Sauter, E. J., Schlüter, M., Klages, M., Foucher, J. P., and Boetius, A.: Novel microbial communities

BGD
10, 8159–8201, 2013

of the Haakon Mosby mud volcano and their role as a methane sink, Nature, 443, 854–858, doi:10.1038/nature05227, 2006.
Orcutt, B. and Meile, C.: Constraints on mechanisms and rates of anaerobic oxidation of methane by microbial consortia: process-based modeling of ANME-2 archaea and sulfate reducing bacteria interactions, Biogeosciences Discuss., 5, 1933–1967, doi:10.5194/bgd-5-1933-2008, 2008.
Orcutt, B., Samarkin, V., Boetius, A., and Joye, S.: On the relationship between methane production and oxidation by anaerobic methanotrophic communities from cold seeps of the Gulf of Mexico, Environ. Microbiol., 10, 1108–1117, 2008.
Peckmann, J., Reimer, A., Luth, U., Luth, C., Hansen, B. T., Heinicke, C., Hoefs, J., and Reitner, J.: Methane-derived carbonates and authigenic pyrite from the northwestern Black Sea, Mar. Geol., 177. 129–150. 2001.
Ranero, C. R. and Von Huene, R.: Subduction erosion along the Middle America convergent margin, Nature, 404, 748–52, doi:10.1038/35008046, 2000.
Reitner, J., Peckmann, J., Blumenberg, M., Michaelis, W., Reimer, A., and Thiel, V.: Concretionary methane-seep carbonates and associated microbial communities in Black Sea sediments, Palaeogeogr. Palaeocl., 227, 18–30, doi:10.1016/j.palaeo.2005.04.033, 2005.
Scambelluri, M., Malaspina, N., and Hermann, J.: Subduction fluids and their interaction with the mantle wedge?: a perspective from the study of high-pressure ultramafic rocks, Period. Mineral., 76, 253–265, doi:10.2451/2007PM0028, 2007.
Schmidt, M., Hensen, C., Mörz, T., Müller, C., Grevemeyer, I., Wallmann, K., Maub, S., and Kaule, N.: Methane hydrate accumulation in “Mound 11” mud volcano, Costa Rica forearc, Mar. Geol., 216, 83–100, 2005.
Schoell, M.: Multiple origins of methane in the Earth, Chem. Geol., 71, 1–10, doi:10.1016/0009-2541(88)90101-5, 1988.
Spiker, E. C. and Hatcher, P. G.: Carbon isotope fractionation of sapropelic organic matter during early diagenesis, Org. Geochem., 5, 283–290, 1984.
Suess, E.: Gashydrat – Eine Verbindung aus Methan und Wasser, Nova Acta LC, 85, 123–146, 2002.
Suess, E.: Handbook of hydrocarbon and lipid microbiology, edited by: Timmis, K. N., Springer-Verlag, Berlin, Heidelberg, 2010.

BGD
10, 8159–8201, 2013

Teichert, B. M. A., Bohrmann, G., and Suess, E.: Chemoherms on Hydrate Ridge – unique microbially mediated carbonate build-ups growing into the water column, Palaeogeogr. Palaeocl., 227, 67–85, 2005.

Thauer, R. K.: Biochemistry of Methanogenesis: a Tribute to Marjory Stephenson, Microbiology, 144, 2377–2406, 1998.

Tishchenko, P., Hensen, C., Wallmann, K. and Wong, C. S.: Calculation of the stability and solubility of methane hydrate in seawater, Chem. Geol., 219, 37–52, 2005.

Torres, M. E., Wallmann, K., Tréhu, A. M., Bohrmann, G., Borowski, W. S., and Tomaru, H.: Gas hydrate growth, methane transport, and chloride enrichment at the southern summit of Hydrate Ridge, Cascadia margin off Oregon, Earth Planet. Sci. Lett., 226, 225–241, doi:10.1016/j.epsl.2004.07.029, 2004.

Treude, T., Boetius, A., Knittel, K., Wallmann, K., and Barker Jørgensen, B.: Anaerobic oxidation of methane above gas hydrates at Hydrate Ridge, NE Pacific Ocean, Mar. Ecol.-Prog. Ser., 264, 1–14, doi:10.3354/meps264001, 2003.

Treude, T., Kru, M., and Jørgensen, B. B.: Environmental control on anaerobic oxidation of methane in the gassy sediments of Eckernförde Bay (German Baltic), Limnol. Oceanogr., 50, 1771–1786, 2005.

Wallmann, K., Drews, M., Aloisi, G., and Bohrmann, G.: Methane discharge into the Black Sea and the global ocean via fluid flow through submarine mud volcanoes, Earth Planet. Sci. Lett., 248, 545–560, doi:10.1016/j.epsl.2006.06.026, 2006.

Wallmann, K., Aloisi, G., Haeckel, M., Tishchenko, P., Pavlova, G., Greinert, J., Kutterolf, S., and Eisenhauer, A: Silicate weathering in anoxic marine sediments, Geochim. Cosmochim. Ac., 72, 2895–2918, doi:10.1016/j.gca.2008.03.026, 2008.

BGD
10, 8159–8201, 2013

Table 1. Overview of sampled stations at Mound 11 and 12 during cruises SO206, SO173/4, M66/3a, and M54/3a.

Site	Station	Instrument	Lat. °N	Lon. °W	Water depth (m)
Mound 11	SO206-38	GC	8°55.36′	84°18.22′	1016
Mound 11	SO206-39	TV-MUC	8°55.34′	84°18.23′	1005
Mound 11	SO206-50	GC	8°55.33′	84°18.23′	1003
Mound 11	M54-155	GC	8°55.36′	84°18.23′	1018
Mound 12	SO206-44	TV-MUC	8°55.69′	84°18.79′	1007
Mound 12	SO206-46	TV-MUC	8°55.72′	84°18.83′	1009
Mound 12	M54-97-2	GC	8°55.90′	84°18.70′	1001
Mound 12	SO173 110-1	GC	8°55.74′	84°18.81′	1008
Mound 12	M66-213	GC	8°55.85′	84°18.60′	980

BGD
10, 8159–8201, 2013

Table 2. List of carbonate samples from Mound 11 and 12 used for mineralogy and stable isotope analysis of carbonates. Samples from SO173, M66, and M54 were used for $^{87}Sr/^{87}Sr$ and $\delta^{13}C$ analysis. (cm b.s.f. = centimeters below seafloor).

Site	Station	Depth (cm b.s.f.)
Mound 11	SO206-38	172–185
Mound 11	SO206-39	8
Mound 11	SO206-39	10–12
Mound 11	SO206-39	11
Mound 11	SO206-39	20–25
Mound 11	SO206-39	26–30
Mound 11	SO206-39, shell	25
Mound 11	SO206-39, shell	26–30
Mound 11	M54-155 A	90
Mound 11	M54-155 B	100
Mound 12	SO206-44	5–8
Mound 12	SO206-46	6–7
Mound 12	SO173-110-1	50–60
Mound 12	M66-213	0
Mound 12	M54-97-2	353
Mound 12	M54 97-2	353

BGD
10, 8159–8201, 2013

Table 3. Summary of model input parameters used for numerical modeling of biogeochemical processes at Mound 11 and 12.

Parameter	Mound 11, SO206-39	Mound 11, SO206-50	Mound 12, SO206-44	Mound 12, SO206-46	Unit	Parameter source
Model parameter values						
Length core	35.5	290	13	9	cm	measured
Length of simulated sediment column	100	500	100	100	cm	fitted
Number of model layers	150	150	150	150		fitted
Temperature	8	8	8	8	°C	measured
Salinity	35	35	35	35	PSU	measured
Pressure	101	101	101	101	bar	measured
Porosity at sediment surface	0.84	0.65	0.76	0.82		measured
Porosity at infinite sediment depth	0.66	0.68	0.68	0.68		fitted
Attenuation coefficient for porosity decrease with depth	0.04	0	0.12	0.16	cm^{-1}	fitted
Coefficient for tortuosity calculation	1	1	1	1		fitted
Burial velocity at depth	0.02	0.02	0.02	0.02	$cm\,yr^{-1}$	fitted
Fluid flow at the sedimet/ water interface	50	1.2	8	15	$cm\,yr^{-1}$	fitted
Kinetic constant for the anaerobic oxidation of methane	1300	100	4000	1000	$mmol\,cm^{-3}\,yr^{-1}$	fitted
Kinetic constant for $CaCO_3$ precipitation	50	0.85	80	500	yr^{-1}	fitted
Density of pore water	1.03184	1.03184	1.03184	1.03184		calculated
Density of dry solids in sediment	2.5	2.5	2.5	2.5	$g\,cm^{-3}$	measured
Kinetic constant for H_2S removal from pore water	0.001	0.0005	0	0	$mmol\,cm^{-3}\,yr^{-1}$	fitted
Attenuation coefficient for decrease in H_2S removal rate	0.001	0	0.00002	0	cm^{-1}	fitted
Non-local mixing coefficient	5	1.2	50	250	yr^{-1}	fitted
Depth of irrigated layer	2	20	1.5	0	cm	fitted
Width of irrigated layer	2	30	0.8	2	cm	fitted
Pore water concentration upper/lower boundary						
BW SO_4^{2-}/BS SO_4^{2-}	27/0	28.5/0	28.5/0	28.5/0	mM	measured
BW CH_4/BS CH_4	0.00001/75	0.00001/85	0.00001/85	0.00001/85	mM	measured
BW Cl^-/BS Cl^-	548/200	550.5/10	557.5/550	550.5/550	mM	measured
BW HCO_3^-/BS HCO_3^-	2.3/4.5	4.0/0	2.3/30	2.3/30	mM	calculated

BW indicates concentrations of dissolved species at the upper boundary of the model column, whereas BS represent concentrations at the bottom of the sediment column.

BGD
10, 8159–8201, 2013

Table 4. Ex-situ determinated rates of anaerobic oxidation of methane (AOM) and sulfate reduction (SR) obtained from SO206 MUC sediment cores, in comparison with previous studies. Modeled AOM rates and benthic fluxes are also presented. All rates are expressed in mmol m^{-2} d^{-1}. Standard deviations (SD) are given.

Site	Station	AOM	SRR	Depth of integration (cm)	AOM	$CaCO_3$ precipitation	SO_4^{2-*}	CH_4^*	TC*	Ca^{2+*}	Simulated core length (cm)
		measured			modeled						
Mound 11	SO206-39	140.71 (±40.84 SD)	117.25 (±82.06 SD)	0–10	188.30	1.29	188.93	−675.26	−237.73	−104.52	100
Mound 11	SO206-50	0.13 (±0.06 SD)	1.47 (±1.81 SD)	0–270	15.92	6.11	15.92	−3.32	−3.67	4.00	500
Mound 12	MUC 44	22.37 (±0.85 SD)	23.99 (±5.79 SD)	0–10	127.29	13.26	127.34	−14.93	−150.55	3.34	100
Mound 12	MUC 46	10.68 (±3.53 SD)	64.97 (±6.79 SD)	0–10	161.62	15.29	161.64	−124.49	−232.05	−13.45	100
Mound 12[1]		16.11		0–10							
Mound 11modeled[2]		9.64		0–27.5							
Hydrate Ridge[3]		99.00 (±102.00 SD)	65.00 (±58.00 SD)	0–10							
Håkon Mosby[4]		19.45 (±5.48 SD)		0–10							

Linke et al., 2000[1]; Karaca et al., 2010[2]; Treude et al., 2003[3]; Niemann et al., 2006[4]
* Total benthic flux, negative values indicate upward flux from sediment into the water column, while positive values represent downward flux from the water column into.

BGD
10, 8159–8201, 2013

Table 5. Mineralogy and stable isotope composition of carbonate samples from Mound 11 and 12 (cruise SO206). Italic highlights samples of bivalve shell fragments. Standard deviations (SD) of laboratory standard (n = 7) are given.

Site	Station	Depth (cm b.s.f.)	carbonate content (weight %)	Dominant carbonate phase	δ^{13}C	SD	δ^{18}O	SD
Mound 11	SO206-38	172–185	82	Mg calcite	−27.1	0.02	5.6	0.04
Mound 11	SO206-39	8	82	Mg calcite	−26.2	0.02	5.9	0.04
Mound 11	SO206-39	10–12	73	Mg calcite	−21.2	0.02	4.7	0.04
Mound 11	SO206-39	11	82	Mg calcite	−27.5	0.02	5.7	0.04
Mound 11	SO206-39	20–25	75	Mg calcite	−29.6	0.02	6.1	0.04
Mound 11	SO206-39	26–30	71	Aragonite	−29.0	0.02	5.8	0.04
Mound 11	*SO206-39, shell*	*25*	*51*	*Aragonite*	*−6.9*	*0.02*	*3.5*	*0.04*
Mound 11	*SO206-39, shell*	*26–30*	*59*	*Aragonite*	*−9.6*	*0.02*	*3.9*	*0.04*
Mound 12	SO206-44	5–8	77	Mg calcite	−48.9	0.02	4.1	0.04
Mound 12	SO206-46	6–7	77	Mg calcite	−45.7	0.02	4.5	0.04

BGD
10, 8159–8201, 2013

Table 6. List of $^{87}Sr/^{86}Sr$ ratios and $\delta^{13}C$ carbonates obtained from Mound 11 and 12 (cruise M54, M66, and SO173). Standard errors (2σ) and Standard deviations (SD) are given.

Site	Station	Depth (cm b.s.f.)	$^{87}Sr/^{86}Sr$	2σ	$\delta^{13}C$	SD	Mineralogy
Mound 11	M54-155 A	155	0.708829	1.4×10^{-5}	−14.14	0.02	ca. 10 % Aragonite
Mound 11	M54-155 B	155	0.709049	7.0×10^{-6}	−15.57	0.02	ca. 70 % Aragonite
Mound 12	M54-97-2 A	353	0.709167	7.5×10^{-6}	−46.28	0.02	> 98 % Aragonite
Mound 12	M54-97-2 B	353	0.709164	6.1×10^{-6}	−46.87	0.02	> 98 % Aragonite
Mound 12	M66-3 213 A	0	0.70909	7.0×10^{-6}	−39.53	0.02	ca. 95 % Aragonite
Mound 12	M66-3 213 B	0	0.709158	8.0×10^{-6}	−42.46	0.02	> 98 % Aragonite
Mound 12	SO173 110-1a	50–60	0.709114	2.1×10^{-5}	−49.13	0.02	ca. 90 % Aragonite
Mound 12	SO173 110-1b	50–60	0.709098	8.0×10^{-6}	−48.61	0.02	> 98 % Aragonite
Mound 12	SO173 110-1(6 A	50–60	0.709088	7.0×10^{-6}	−47.50	0.02	> 98 % Aragonite
Mound 12	SO173 110-1(6 B	50–60	0.709097	6.0×10^{-6}	−48.58	0.02	> 98 % Aragonite
Modern seawater*			0.709176	1.5×10^{-5}			

* IAPSO standard seawater was used to represent modern seawater $^{87}Sr/^{86}Sr$ ratio.

BGD
10, 8159–8201, 2013

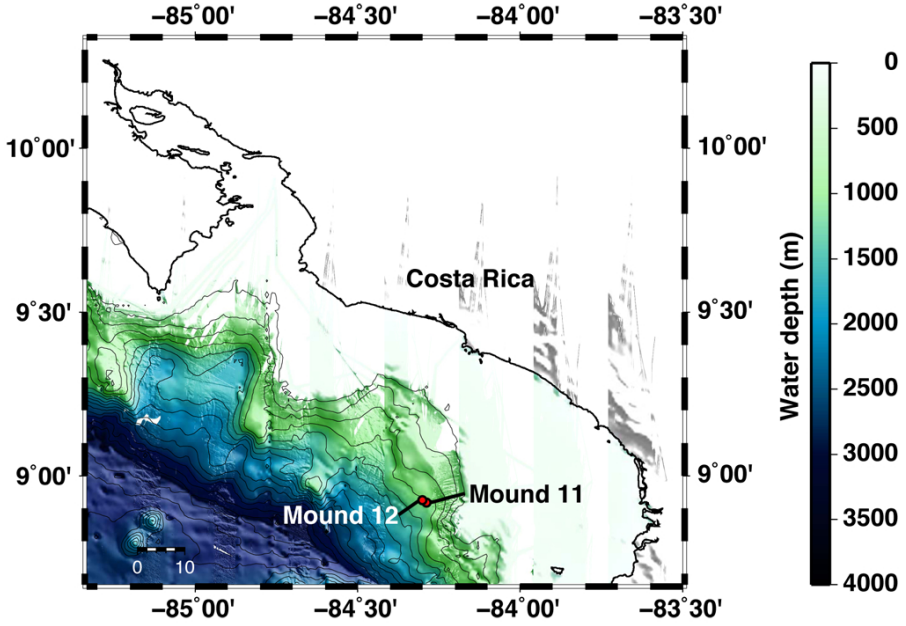

Fig. 1. Bathymetric map of the pacific continental slope of Costa Rica, locations Mound 11 and Mound 12 are indicated.

BGD
10, 8159–8201, 2013

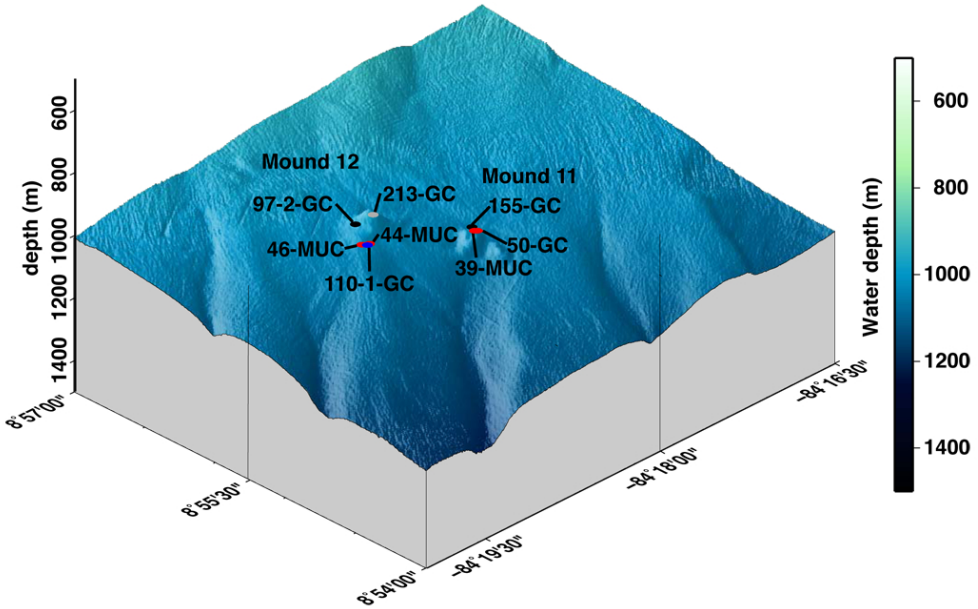

Fig. 2. 3-dimensional relief map of the study area offshore Costa Rica showing stations at Mound 11 and 12 sampled during SO206 (red), SO173 (blue), M66 (grey), and M54 (black).

BGD
10, 8159–8201, 2013

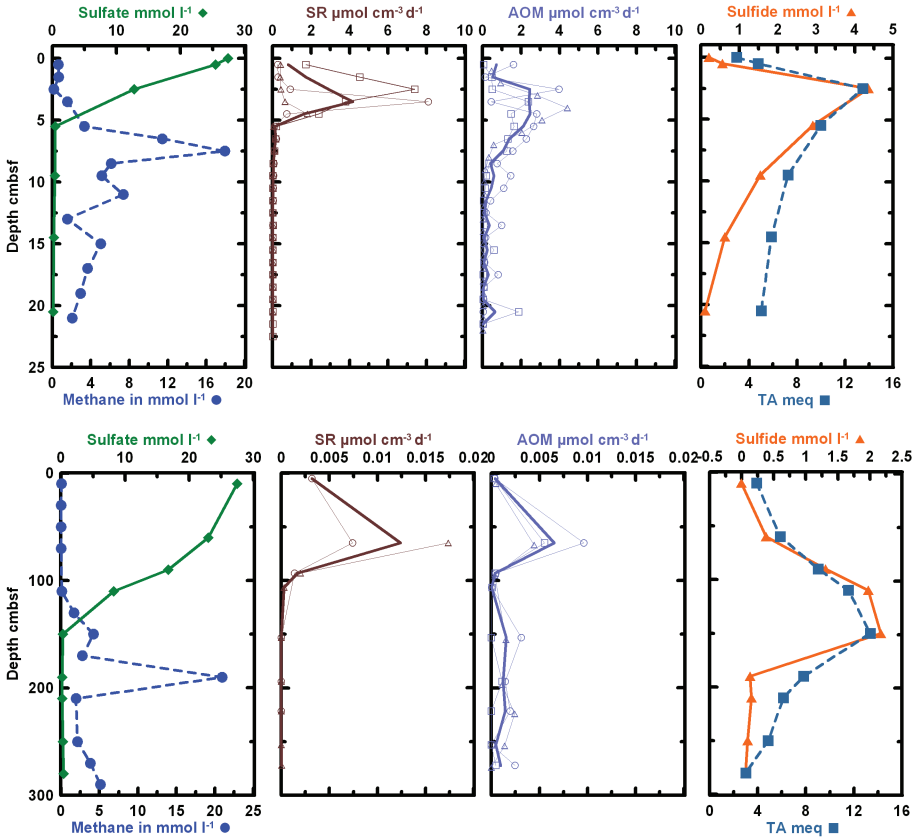

Fig. 3. Mound 11 porewater profiles for sulfate, methane, sulfide, and total alkalinity (TA) as well as sediment rates of sulfate reduction (SR) and anaerobic oxidation of methane (AOM). Top: MUC 39 (covered by sulfur bacteria mat), bottom: GC 50. For SR and AOM profiles of individual replicates (fine lines with symbols) average profiles (bold lines w/o symbols) are given.

BGD
10, 8159–8201, 2013

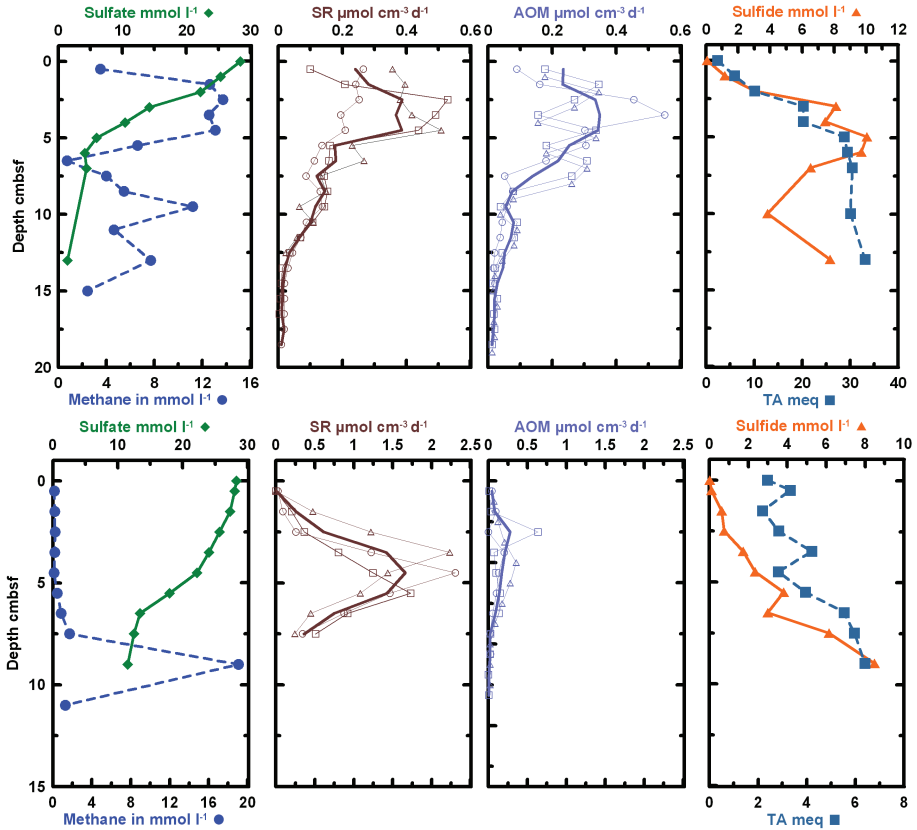

Fig. 4. Mound 12 porewater profiles for sulfate, methane, sulfide, and total alkalinity (TA) as well as sediment rates of sulfate reduction (SR) and anaerobic oxidation of methane (AOM). Top: MUC 44 (covered by sulfur bacteria mat), bottom: MUC 46 cores (covered by bacterial mat). For SR and AOM profiles of individual replicates (fine lines with symbols) average profiles (bold lines w/o symbols) are given.

BGD
10, 8159–8201, 2013

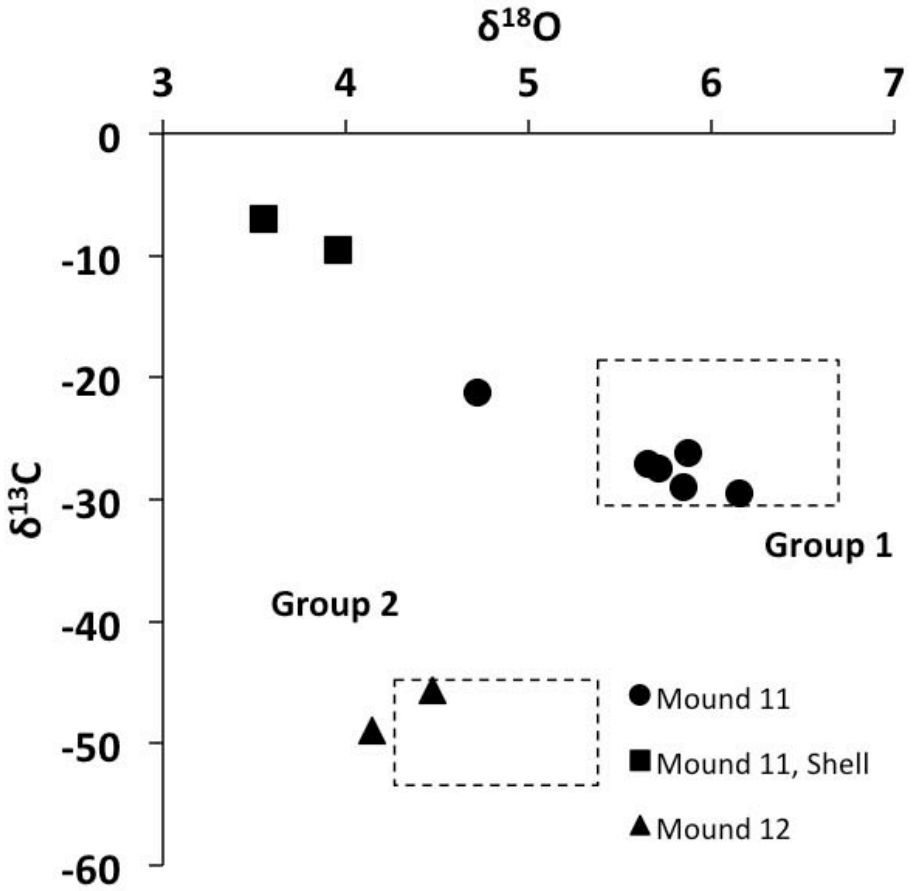

Fig. 5. δ^{13}C vs. δ^{18}O plot of carbonate material sampled from various locations during SO206 (solid symbols). Grouping, based on isotopic, petrographic, mineralogical, and morphological similarities was carried out according to Han et al. (2004). All values referred to the V-PDB scale.

BGD
10, 8159–8201, 2013

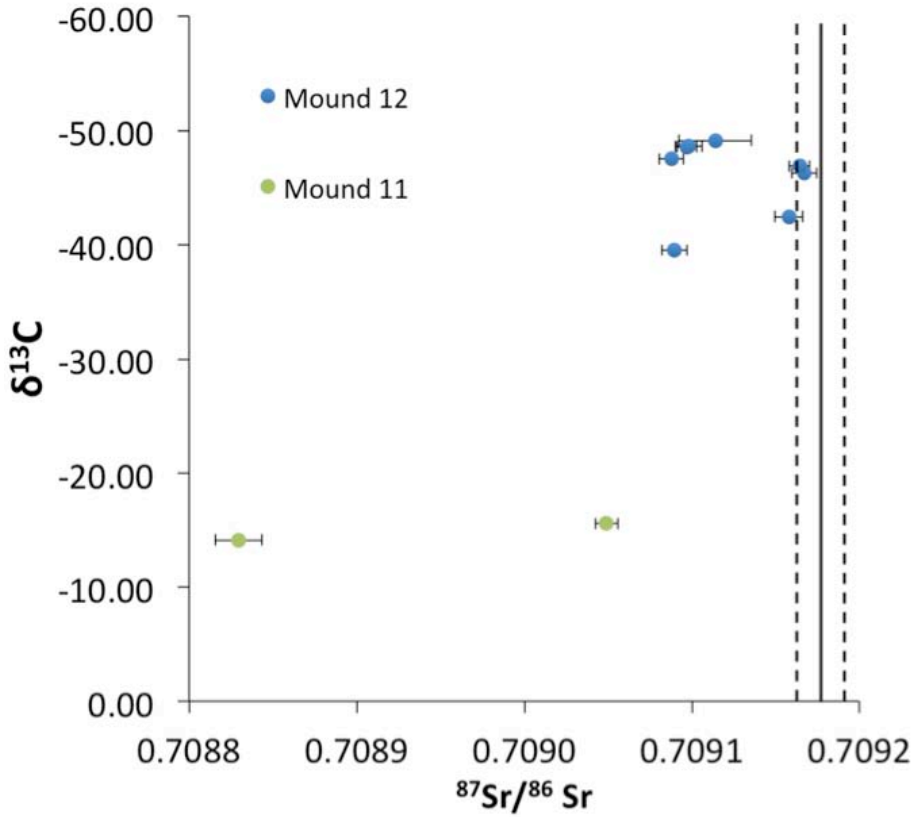

Fig. 6. δ^{13}C vs. ^{87}Sr/^{86}Sr ratios of carbonate material sampled during cruises SO173/4, M66/3a, and M54/3a. Second Standard Errors (2σ) of individual ^{87}Sr/^{86}Sr measurements are given. The solid line indicates the measured ^{87}Sr/^{86}Sr ratio of IAPSO standard seawater; dotted lines represent Second Standard Error (2σ). Standard deviation of δ^{13}C measurements was 0.02 ‰ (symbols larger than error bars).

BGD
10, 8159–8201, 2013